Appl. Phys. A (2017) 123:293
DOI 10.1007/s00339-017-0929-y

Applied Physics A
Materials Science & Processing

Femtosecond laser additive manufacturing of YSZ

Jian Liu[1] · **Shuang Bai**[1]

Received: 7 October 2016 / Accepted: 25 March 2017

Abstract Laser additive manufacturing (LAM) of Yttria-Stabilized Zirconia (YSZ) is investigated using femtosecond (fs) fiber lasers. Various processing conditions are studied, which leads to desired characteristics in terms of morphology, porosity, hardness, microstructural and mechanical properties of the processed components. High-density (>99%) YSZ part with refined grain and increased hardness was obtained. Microstructure features of fabricated specimens were studied with SEM, EDX, the measured micro hardness is achieved as high as 18.84 GPa.

1 Introduction

In recent years, solid oxide fuel cells (SOFC), as energy conversion systems, have been attracted many attentions due to its high efficiency and almost no pollution to the environment [1]. For a typical SOFC system, it generally employs YSZ and Ni/YSZ cermet as the materials for electrolyte and anode composition because of its high catalytic activity, electronic and ionic conductivity as well as stability. As reported [2–5], various methods have been employed for the fabrication of YSZ and Ni/YSZ electrolyte and anode components, such as die pressing, tape casting, gel casting, slip casting, screen printing, wet powder spraying, dip coating, plasma spraying. However, these methods are limited to special part geometry (planar or tubular) manufacturing associated with higher porosity.

Laser additive manufacturing (LAM) [6–11] (e.g., selective laser melting SLM) uses material powders or small parts to build three dimensional parts with complicated structures. It has been proved to be an efficient, robust, and cost effective way for the next generation manufacturing. Though many breakthroughs have been achieved, especially in metals and alloys materials, it is still a big challenge for processing of YSZ powders via LAM, due to YSZ's special properties, such as brittleness, light weight, inherent tendency of fine particles to agglomerate. Direct LAM of YSZ without binders can result in micro cracks, over burned, discontinuity structures, porosity and other defects.

In this paper, for the first time, solid YSZ electrolyte with full densification was successfully made from micro size powders by employing femtosecond laser direct additive manufacturing. A series of process control parameters were systematically studied from line writing and layer melting to optimize final performance, including laser power, scanning speed and hatching space. Microstructure and mechanical properties of the fabricated parts were investigated in details.

2 Experimental setup

A high power mode-locked Yb-doped fiber laser (Laser-Femto, Inc., California), delivering up to 250 W average power at 80 MHz with central wavelength at 1030 nm, was used in the experiments. Output pulses were compressed to have a full-width-half-maximum (FWHM) pulse duration of 800 fs. Laser beam was guided through a galvanic-mirror enabled scanner and raster-scanned on the powder surface. The laser beam was focused by a lens with 100-mm-long focal length and had a FWHM beam diameter of 25 μm on

✉ Jian Liu
jianliu@polaronyx.com

[1] PolarOnyx, Inc., 2526 Qume Drive, Suite 17, San Jose, CA 95131, USA

Published online: 01 April 2017

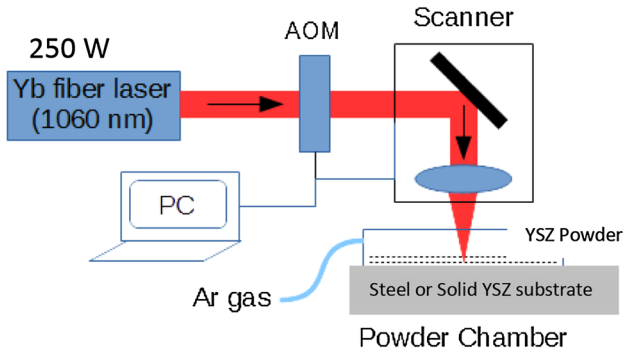

Fig. 1 Schematic of the experimental setup. *AOM* acoustic optical modulator

Table 1 Thermal properties of YSZ powders

Melting temperature (°C)	>2690
Thermal conductivity (W/m.K)	1.7–8.0
Thermal expansion coefficient (μm/m.K)	10.5
Thermal diffusivity (mm^2/s)	0.196–0.352

target. Considering the loss through all the components, the maximum power on powder surface is about 170 W. The laser beam was guided through an acoustic-optical modulator (AOM, Gooch & Housego, Florida, USA), which was used to control the laser on/off and variation of the laser power. The laser scanner was synchronized with the AOM and used to scan the laser beam on the powder surface. The scanner was mounted on a motorized stage to control the focal condition of the laser beam relative to the powder surface. Schematic of experimental setup was shown in Fig. 1.

The Yttria-Stabilized Zirconia (YSZ) powders have a surface area size distribution of 4.5 m^2/g (fuelcellmaterials. Inc, Ohio), thermal properties were presented in Table 1. A few parameters, such as laser power, scanning speed and hatching (line spacing) were varied to optimize YSZ layer melting process. Final manufactured YSZ solid layer surface was characterized with optical microscope, microstructure evolution was analyzed by scanning electron microscope (SEM). Moreover, the cross-sections of the samples were prepared and polished for SEM image. EDX was also conducted on the cross-sections to analyze the element concentrations [10]. Micro hardness was test on the cross-sections for melting performances identification [10].

3 Results and discussion

3.1 Influence of laser power and scanning speed on melting parts morphologies and microstructure

Laser power coupled with scanning speed are the very important process parameters which influence the sintered YSZ layers structure and densification. In this study, at first, the average power of 29.8 W was fixed for line melting, totally 8 specimens were prepared using different laser scanning speed at: 1, 5, 7.5, 10, 20, 50, 75, 100 mm/s. Melting performances influenced by different scanning speed were investigated, correlation to laser shockwave and heating accumulation was studied as well. The melting performance for eight specimens without any post treatment are shown in Fig. 2a–h. It can be clearly seen that at lowest scanning speed of 1 mm/s, along the laser beam scanning direction, YSZ powders are overheated and dendritic melting parts formed due to laser shockwave and YSZ powders comparable good flowability, as shown in Fig. 2a. When laser scanning speed is less than 20 mm/s, overheating is severe and cannot be avoided due to concentrated intensive laser energy accumulation, as shown from Fig. 2b–d. Good melting zone can be found in Fig. 2e, in this case, total laser energy output for melting process was just right enough with no overheating existed. While the laser scanning speed is much larger, total laser energy absorbed for melting process is not enough, unmelt lines can be obviously seen there, as shown from Fig. 2f–h.

Based on the first step tests of line melting analysis, we believe that good big size of YSZ layer melting is challenging but feasible. Figure 3a–d shows the images of the surfaces of the melt YSZ layers without any post treatment. As shown in Fig. 3a–d, under low laser power and scanning speed of melting process, hollow structures are formed with loosed powders and unmelt agglomerated particles. It can be explained that total absorbed laser energy was distributed unevenly in the whole melting area, and also the laser shockwave influence was integrated locally. As a result, the temperature in some places is much higher than other locations, melting is non-uniform in the total area. As the increased laser power and scanning speed, continuous layers can be manufactured as shown in Fig. 3e–g, while it should be notified that penetration holes, inhomogeneous topography with waviness and roughness, micro cracks and other defects are still needed to be improved. The reason for these defects can be attributed to the intensive laser energy concentration in partially and surface tensile residual stress. It can be seen that in Fig. 3h, largest shinning area can be observed, which means the whole melting area is more flat and almost focused at the same level during the imaging of optical microscopy. For this case that large laser power of 131 W and fast scanning speed of 300 mm/s, good melting

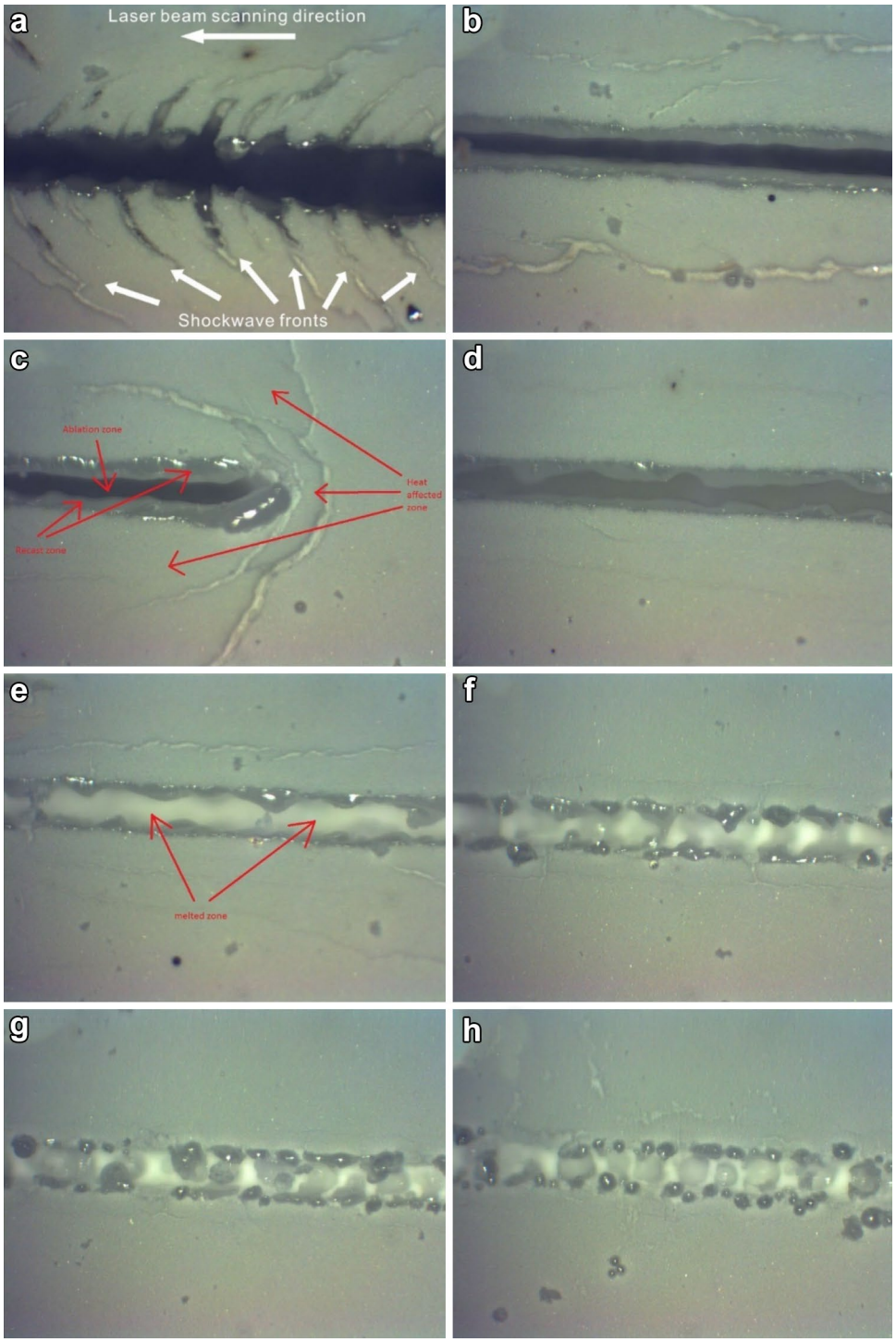

Fig. 2 Line melting performances under different laser scanning speed (no post treatment): **a** 1 mm/s, **b** 5 mm/s, **c** 7.5 mm/s, **d** 10 mm/s, **e** 20 mm/s, **f** 50 mm/s, **g** 75 mm/s, **h** 100 mm/s

layer with fully densification and homogeneous structure with minimum defects was fabricated.

SEM images of layer melting performances under different laser power and scanning speed are presented in Fig. 4. It can be seen that under laser power of 68 W and scanning speed of 80 mm/s processing, microstructure is very tight and uniform with good dislocation density, no obvious porosity existed, as shown in Fig. 4a, b. When keep the same laser of 68 W while scanning speed increased to 100 mm/s, more loose particles and larger amounts of tiny cracks can be found across the surface, as shown in Fig. 4c, d. This can be explained that as the increased of scanning speed, melting is not enough for all of the powders, as a result, thermal distribution across the whole area is more non-uniform, more tiny cracks were formed due to surface tensile residual

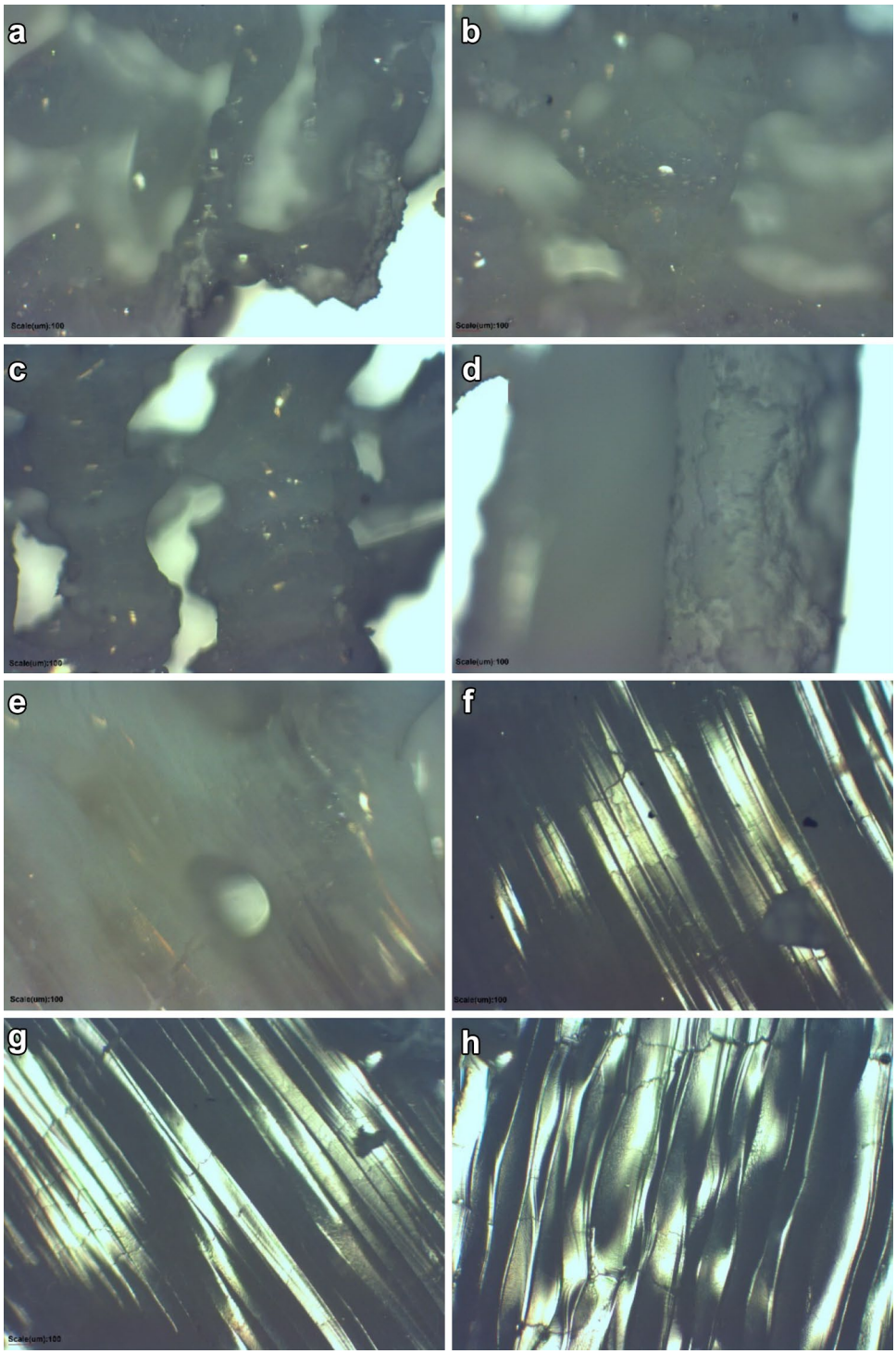

Fig. 3 Microscopy images of melt layer surfaces under different laser power and scanning speed (no post treatment): **a** 28 W, 34 mm/s, **b** 35 W, 34 mm/s, **c** 35 W, 28 mm/s, **d** 37 W, 10 mm/s, **e** 68 W, 80 mm/s, **f** 78 W, 100 mm/s, **g** 78 W, 150 mm/s, **h** 131 W, 300 mm/s

stress and thermal dispatch. When laser power is too low less than 37 W, melting effects becomes much poor, high porosity with loose particles can be easily seen from Fig. 4e, f. In Fig. 4, 50 μm scale bars are used for a, c, e, and 10 μm for b, d, f.

Densification of melting layer under different laser power processing was calibrated by image J, as shown in Fig. 5, the density is significantly improved with the increasing of laser powder, the highest density of 99.5% has been achieved.

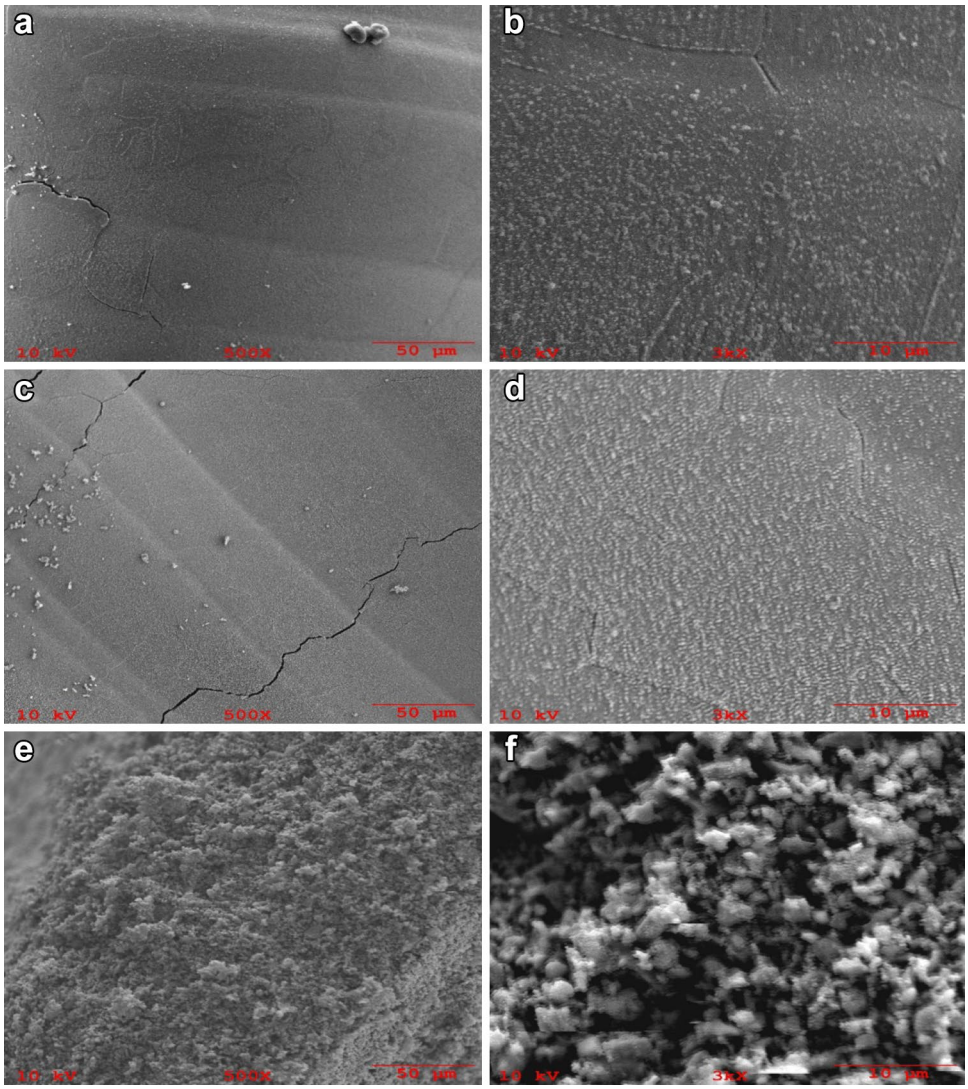

Fig. 4 SEM images of layer melting performances under different laser power and scanning speed: **a, b** 68 W, 80 mm/s, **c, d** 68 W, 100 mm/s, **e, f** 37 W, 10 mm/s. *Scale bars* 50 μm for (**a, c, e**), and 10 μm for (**b, d, f**)

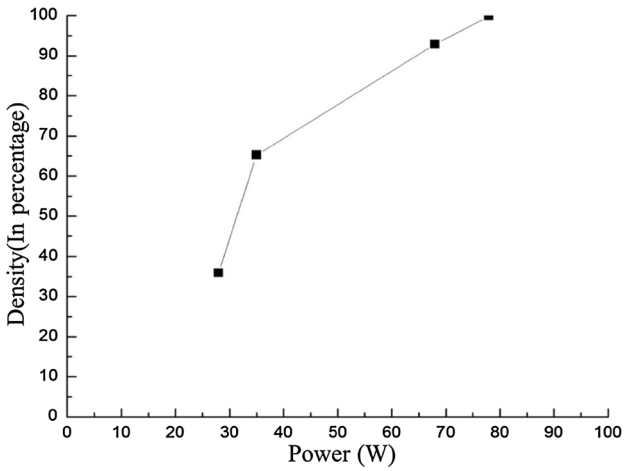

Fig. 5 YSZ melting layer density varies with increased target power

3.2 Influence of hatching space on layer melting morphologies and structure

The dependence of melting quality on hatching (line space) is also investigated. For narrow hatching space of 15 μm, it can be clearly seen from Fig. 6a (melt layer surface without post treatment) that narrow and tight surface waviness with crossed cracks was formed, even more tiny holes dispersed in the whole surface. As the increasing of hatching space, the structures are more smoothly with less cracks, as shown in Fig. 6b. The possible reason is that if line space is too narrow less than laser beam size, overlapped melting process induced the previous solidified parts were re-melt again, partial overheating occurred. When the hatching space is close to laser beam size, the most smooth and densified surface was formed, as shown in Fig. 6c. The ripple line width varies with hatching space was shown in Fig. 7.

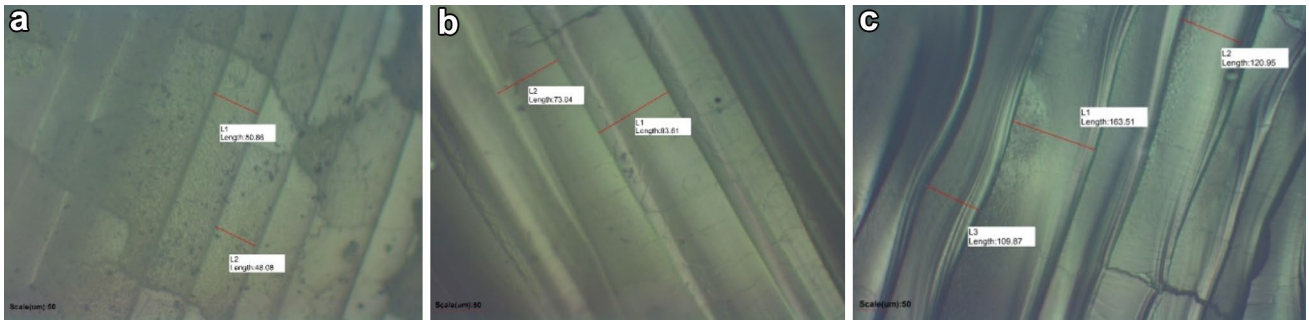

Fig. 6 Microscopy images of melt layer surfaces under different hatching space (no post treatment): **a** 15 µm, **b** 20 µm, **c** 30 µm

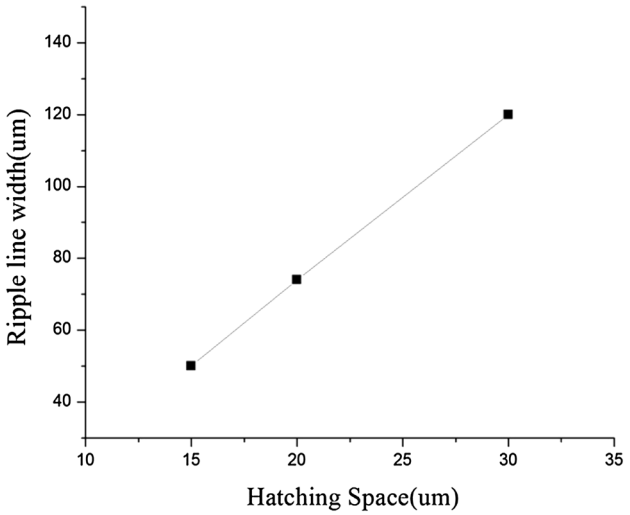

Fig. 7 Texture varies as hatching space

Fig. 8 Picture of good melting layer prepared under laser power of 131 W and scanning speed of 300 mm/s, hatching space of 30 µm

3.3 An example of high quality layer melting part

By elevating the laser power to 131 W and scanning speed to 300 mm/s, the high quality of thin layer melting part with full densification as shown in Fig. 8 is achieved, the total area size is larger than 20×60 mm.

Figure 9 shows the SEM images of the cross section of fully melt YSZ layers, the microstructure is pretty dense and uniform with no porosity is observed, good melting depth as large as 100 µm was achieved. Element analysis of the melted region and original YSZ powders were conducted by EDX (Fig. 9c, d). By eliminating the extra elements (gold for imaging charge and carbon from the mounting media) introduced from the SEM sample preparation, the weight percentage of oxygen and yttrium decreased when compared with original as-received YSZ powders from fuelcellmaterials. Inc, which may result from Yittria decomposition under laser melting process and then reinforced into zirconia lattice matrix.

The measured micro hardness (method is similar to reference [10]) is 18.84 GPa, much larger than the hardness of industrial made granular YSZ solid disk (received from fuelcellmaterials. Inc) which is 13.66 GPa.

4 Conclusion

For the first time, fully melting of YSZ powders was demonstrated via a high-power fs fiber laser additive manufacturing. The processed samples were examined and characterized by optical microscope, SEM, EDX and Knoop hardness test. It shows the microstructure is dense and uniform with the density of larger than 99% and micro hardness of 18.84 GPa achieved. We believe there will be a great potential for semiconductor and energy industries.

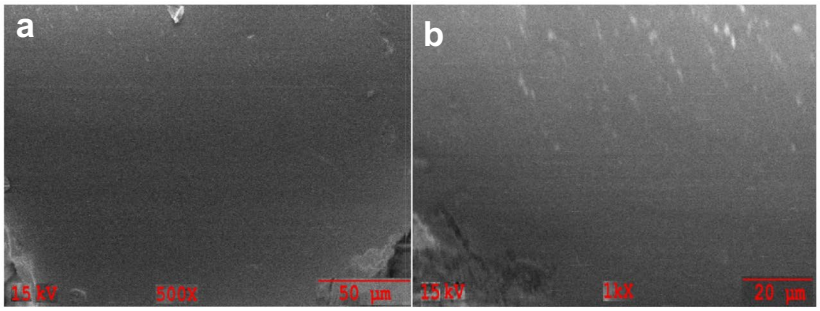

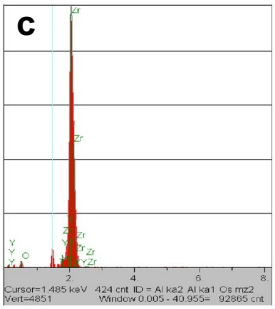

Elt.	Line	Intensity (c/s)	Atomic %	Conc	Units	Error 2-sig	MDL 3-sig	
O	Ka	10.22	17.077	3.489	wt.%	0.230	0.359	
Y	La	19.05	2.826	3.208	wt.%	0.155	0.465	
Zr	La	551.15	80.097	93.303	wt.%	0.838	0.455	
			100.000	100.000	wt.%			Total

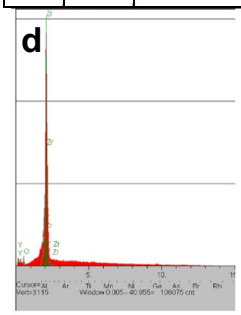

Elt.	Line	Intensity (c/s)	Atomic %	Conc	Units	Error 2-sig	MDL 3-sig	
O	Ka	7.79	9.927	1.901	wt.%	0.158	0.228	
Y	La	43.62	9.369	9.971	wt.%	0.350	0.560	
Zr	La	373.02	80.705	88.128	wt.%	1.058	0.566	
			100.000	100.000	wt.%			Total

Fig. 9 **a** Cross sectional SEM images of the good melted YSZ layer. *Scale bar* 50 µm. **b** High-magnification cross-sectional SEM of the fully melted region as shown in **a**. *Scale bar* 20 µm. **c** EDX result of the fully melted region. **d** EDX result of the original YSZ powders

References

1. N.Q. Minh, Ceramic fuel cells. J. AM. Ceram. Soc **76**, 563 (1993)
2. W.L. Huang, Q. Zhu, Z. Xie, Gel-cast anode substrates for solid oxide fuel cells. J. Power Sources **162**, 464–468 (2006)
3. N.M. Sammes, Y. Du, R. Bove, Design and fabrication of a 100W anode supported micro-tubular SOFC stack. J. Power Sources **145**, 428–434 (2005)
4. V. Lawlor, "Review of the micro-tubular solid oxide fuel cell (Part II:Cell design issues and research activities)". J. Power Sources **240**, 421–441 (2013)
5. J. Ding, J. Liu, W. Yuan, Y. Zhang, Slip casting combined with colloidal spray coating in fabrication of tubular anode-supported solid oxide fuel cells. J Euro. Ceram. Soc **28**, 3113–3117 (2008)
6. L. Greenemeier, NASA plans for 3-D printing rocket engine parts could boost larger manufacturing trend. Scientific American (2012)
7. F. Abe, K. Osakada, M. Shiomi, K. Uematsu, M. Matsumoto, The manufacturing of hard tools from metallic powders by selective laser melting. J. Mater. Process. Technol. **111**, 210–213 (2001)
8. S. Bai, L. Yang, J. Liu, Manipulation of microstructure in laser additive manufacturing. Appl. Phys. A **122**, 495–499 (2016)

9. B. Nie, H. Huang, S. Bai, J. Liu, Femtosecond laser melting and resolidifying of high-temperature powder materials. Appl. Phys. A 118(1), 37–41 (2015)
10. Bai Nie, Lihmei Yang, Huan Huang, Shuang Bai, Peng Wan, Jian Liu, Femtosecond laser additive manufacturing of iron and tungsten parts. Appl. Phys. A 119(3), 1075–1080 (2015)
11. B. Fulcher, Effects of laser parameter variation and thermal processing on mechanical properties and microstructure of laser-melted Inconel 718, Paper 1146, Additive Manufacturing with Powder Metallurgy Conference (Orlando, 2014)